Received: 7 May 2021 | Revised: 16 June 2021 | Accepted: 19 June 2021

DOI: 10.1002/aoc.6355

RESEARCH ARTICLE

Applied Organometallic Chemistry WILEY

Visible light photodegradation of 4-nitrophenol by new high-performance and easy recoverable Fe_3O_4/Ag_2O-LDH hybrid photocatalysts

Mohammad Dinari | **Firooze Dadkhah**

Department of Chemistry, Isfahan University of Technology, Isfahan, Iran

Correspondence
Mohammad Dinari, Department of Chemistry, Isfahan University of Technology, Isfahan 84156-83111, Iran.
Email: dinari@iut.ac.ir; mdinary@gmail.com

Funding information
Research Affairs Division Isfahan University of Technology (IUT)

Abstract

Till now, water contaminant photodegradation has been the most influential method to remove low but dangerous concentrations of pollutants. Herein, a green method was employed to enhance the photocatalytic activity of ZnAl-LDH through depositing Ag and magnetite nanoparticles on the surface of layered double hydroxide (LDH) sheets. The structural and electrochemical characterization of as-prepared Zn_3Al-CO_3 (ZA-LDH) and Fe_3O_4/Ag_2O-LDH ($M_{10}A_5$-LDH) composite was determined by X-ray diffraction (XRD) analysis, Brunauer–Emmett–Teller (BET) theory, field emission scanning electron microscopy (FESEM) along with energy-dispersive X-ray spectroscopy (EDX) mapping, UV–vis diffuse reflectance spectra, photoluminescence spectra, and transient photocurrent response. All of the analyses confirmed the photo-response enhancement of the $M_{10}A_5$-LDH compared with virgin LDH. The mineralization of *p*-nitrophenol (PNP) under visible light revealed that the photodegradation rate of composite (0.02 min^{-1}) is fourfold more significant than that of the bare ZA-LDH (0.005 min^{-1}). The active radical capturing tests exhibited that h^+, •OH, and $•O_2^-$ play substantial roles in PNP degradation, respectively. The potential photodegradation mechanism involves the charge transfer from Fe_3O_4 and Ag_2O to LDH, producing active radicals for the degradation process.

KEYWORDS

4-nitrophenol, easy recoverable, Fe_3O_4/Ag_2O-LDH, magnetic nanocomposite, photodegradation

1 | INTRODUCTION

As the most toxic mono-nitrophenol, 4-nitrophenol (4-NP) is a severe threat to ecological systems, and even 20 mg L^{-1} of it could raise the risk of cancer.[1] The most common sources of 4-NP in wastewaters are pesticides, medicines, dyes, explosives, leather coloring agents, and plastics.[2,3] It also can deposit in the soil as a hydrolysis product of organophosphorus insecticides like parathion and methyl parathion.[4] To minimize the amount of 4-NP in the environment, many different techniques with chemical, biological, and physical approaches were developed. Even though all the accomplishments have been made using these technologies, high-energy consumption, secondary contamination, and low proficiency are the weaknesses of these methods. Therefore, advanced oxidation processes (AOPs) are introduced as an alternative, which has no harmful product, has no expensive

oxidants needed, and at the same time has other advantages like complete mineralization, low cost, and mild conditions.[5–7] The key to achieving the best efficiency of this technology is to develop high-performance photocatalytic materials with high catalytic activity, reasonable stability, easy recyclability, and green solar energy as a driving force.[8,9] Nowadays, solar light semiconductor photocatalysts have drawn attention as the cheapest light source needed in wastewater treatment. Although more familiar photocatalysts based on TiO_2,[10] carbon nanotubes,[11] zinc oxide,[12] and metal oxides[13] were investigated, recently, layered double hydroxide (LDH)-based photocatalysts with extended properties like adjustable composition, accessible active sites, excellent dispersions, and especially synergistic effects with other materials offered brand new photocatalysts in pollutant degradation.[14–16] Compared with single-phase photocatalyst, component tunability of LDH not only allows each material to keep its characteristic but also promotes the performance of the catalyst through expanding the gap between the hole and photoexcited electron and thus stretch the scope of light absorption.[17] In addition, by adjusting influential factors in LDH structure such as structural metals (Zn, Co, and Ni) and interlayer anion (CO_3, NO_3, etc.) and turning LDH to mixed metal oxides, properties like band gap, pollutant adsorption capacity, specific surface area, and thus the level of the photocatalytic activity are controllable.[18] However, to adjust the wide band gap of the LDH and increase the delay in electron–hole recombination, some modifications are needed.[19]

One of the solutions to upgrade the photocatalytic activity is to design a hybrid system. A composite constructed from a wide band gap semiconductor like LDH and a narrow band gap metal/metal oxide semiconductor interacts with each other. As a result, the holes left over from photoexcited electrons traps in metal/metal oxide semiconductors. The photoexcited electrons transfer to the LDH under the illumination of light, thus decreasing the speed of electron–hole recombination and enhancing the charge separation.[20]

Different iron oxide types as n-type semiconductors can be synthesized at a low cost and show photoactivity in organic contaminant degradation reactions.[21,22] Fe_3O_4 has not only superior magnetism but also a narrow band gap to transfer photogenerated electrons rapidly.[23] The electrons can hop between crystal field bands of octahedral and tetrahedral sites at room temperature, which allows referring magnetite to an important class of half-metallic materials.[24,25] Thus, magnetic composites can be removed from the medium and reused easily and show good photocatalytic performance as well. Another useful strategy to improve photocatalytic efficiency is to construct a noble metal-loaded composite. The reason is that the surface plasmon resonance (SPR) phenomenon of noble metals can enhance the visible light absorption capacity of the photocatalyst. Silver oxides (AgO and Ag_2O) can potentially absorb visible light due to their ideal band gap and bring a more effective charge transfer interface and holes in comparison with the traditional composites.[26] Additionally, thermodynamic stability and low toxicity make them good candidates for organic pollutant degradation.[27–29]

In this work, to fabricate an environmentally safe and highly efficient visible light responsive photocatalyst, a magnetic composite was engineered. To raise the visible light absorption of catalyst, the ZA-LDH was synthesized with CO_3 interlayer anion, calcinated at 500°C, and the amount of Fe_3O_4 and Ag_2O regulated. First, the structural and photoelectrochemical characteristics of ZA-LDH and M_xA_5-LDH photocatalysts were studied. Next, the photocatalytic performance of composite was evaluated by the mineralization of *p*-nitrophenol (PNP). The possible mechanism of PNP photodegradation is pictured based on the trapping experiment of the active radicals.

2 | MATERIALS AND METHODS

2.1 | Chemicals

Primary materials such as Zn $(NO_3)_2{\cdot}6H_2O$, Al $(NO_3)_3{\cdot}9H_2O$, Na_2CO_3, NaOH, $AgNO_3$, PNP, and other chemicals needed for the synthesis of magnetite ($FeCl_3{\cdot}6H_2O$, $FeCl_2{\cdot}4H_2O$, and ammonia) had analytical-grade purity and purchased from Merck or Aldrich company.

2.2 | Photocatalytic synthesis

The Zn_3Al-CO_3 LDH was synthesized as host–guest layered material by the coprecipitation method. After preparation of an aqueous solution containing Zn $(NO_3)_2{\cdot}6H_2O$ and Al $(NO_3)_3{\cdot}9H_2O$ with mol ratio of Zn/Al: 3, the pH of the solution was adjusted to 10 by simultaneous slow injection of Na_2CO_3 and NaOH solutions. The resulting white precipitate was stirred vigorously for 24 h at 80°C. After the separation of colloidal suspension by centrifugation, the wet LDH was calcinated at 500°C for 6 h in the air to obtain a mixture of metal oxides and labeled as ZnAl-LDO.[30,31] Furthermore, M_xA_5-LDH photocatalyst was synthesized by the use of the reconstruction ability of the LDH layers. Briefly, after suspending a certain amount of magnetite, which was synthesized based on our previous work,[32]

LDO powder was added to that. An aqueous solution of $AgNO_3$ was added to the mixture, although the ratio of Ag/LDH was fixed at 5% wt. The continuous stirring for 12 h promoted the complete reconstruction of LDH and embedded Ag and magnetite in its structure. Then, an aqueous solution of urea was injected to establish the formation of Ag_2O at 60°C for 4 h. The final product was collected by an external magnet. Two photocatalysts were synthesized with 10% and 15% of magnetite content ($M_{10}A_5$-LDH and $M_{15}A_5$-LDH).

2.3 | Instrumentation

To uniform magnetite, an ultrasonic homogenizer device (100 W–25 Hz) is used. The chemical composition and crystalline structures of the catalysts were determined using an X-ray diffraction (XRD) analysis at $2\theta = 10–80°$ on Bruker Nanostar X-ray powder diffractometer with Cu Kα radiation at the wavelength ($\lambda = 0.1542$ nm). Brunauer–Emmett–Teller (BET) theory characterized nitrogen adsorption on a specific surface area at 77 K using the BELSORP-mini II device (BEL Japan, Inc.). The morphologies of the samples are analyzed by field emission scanning electron microscopy (FESEM; Tescan Mira3, Czech Republic) with energy-dispersive X-ray spectroscopy (EDX) for the determination of metal composition. The photoluminescence (PL) spectra were indicated the recombination of electron holes using the Cary Eclipse (MY13250011) instrument with a 520 V PMT. Diffuse reflection spectroscopy (DRS) examines the interaction of light with matter using the V-670 device (UV-VEs, Japan). A deuterium lamp for ultraviolet (UV) light and a tungsten halogen lamp for visible were utilized as a light source and working range of 195–1100 nm. UV–vis spectra were monitored with a wavelength ranging from 250 to 500 nm using a Shimadzu UV–vis 2600 double beam spectrophotometer. A 400-W metal halide lamp was used as the light source in photodegradation tests. The transient photocurrent (TPC) measurements were carried out using a three-electrode quartz cell with 0.1 mol L^{-1} Na_2SO_4 electrolyte solution at room temperature.

2.4 | Photocatalytic run

The photocatalytic measurements were carried out with ZA-LDH, $M_{10}A_5$-LDH, and $M_{15}A_5$-LDH dispersed in a 100-mL aqueous solution of 10 ppm PNP. Before the reaction, the mixture was vigorously stirred for 15 min to reach dark-adsorption equilibrium. Photocatalytic degradation experiments were conducted in a photocatalytic system, including a 400-W metal halide lamp as a visible light source and a cooling system to maintain the temperature at room temperature. Then, the visible light source was switched on, whereas the lamp was set at a 10-cm distance from the sample. Samples were taken for 180 min every 30 min, and after removing the catalyst by an external magnet, the solution was analyzed utilizing a UV–vis spectrophotometer at λ_{max} of 400 nm. Also, the PNP contaminant solution was sampled in the same period in dark conditions as a blank test.

3 | RESULTS AND DISCUSSION

3.1 | Characterization of the photocatalyst

The crystalline and phase structures of all the samples were collected, as presented in Figure 1. The diffractogram of the pure ZnAl LDH was inconsistent with previous reports.[33,34] The sharp basal diffraction peaks at $2\theta = 11.8°$ and 23.5° are related to (003) and (006) planes and show high crystallinity of the sample (Figure 1a). The interlayer distance of 0.76 nm is a sign of CO_3^{2-} as the intercalated anion (JCPDS 38-0486). However, the crystalline structure was destroyed through the calcination of abovementioned LDH at 500°C and ZnO with close-packed hexagonal (wurtzite) structure formed, whereas no diffraction peak related to Al was observed (Figure 1b). The reason could be the existence of the amorphous phase Al ion in the center of the zinc oxide structure.[35,36] The XRD pattern of the $M_{10}A_5$-LDH is represented in Figure 1c. Besides the diffraction peaks of reconstructed LDH in composite, the result confirms the coexistence of Fe_3O_4 and Ag_2O in magnetite/Ag_2O-LDH composites. The Miller planes related to the magnetite phase were (220), (311), (400), (422), (511), and (440) and correspond approximately to angles at 30°, 35°, 43° 53°, 56°, and 62°, respectively. The most diffraction peaks of Ag_2O interfered with magnetite. However, peaks that appeared around 53.2° and 65.7° are related to the [220] and [311] Ag_2O plans (JCPDS 41-1104).[32] The comparison between the XRD patterns of virgin LDH and composite exhibits no peak shift, implying that the crystal structure had no change after introducing magnetite and Ag_2O into the crystal lattice of LDH.[37]

Also, the calculation of the lattice parameter "a" based on the reflection of (110) plane for both pure LDH and composite, as it describes the intercation distance within the hydroxide layers, shows no distinguishable differences between the intercation distance after deposition of the Ag_2O and Fe_3O_4 NPs (Table 1). This indicates the complete reconstruction of brucite-like LDH sheets

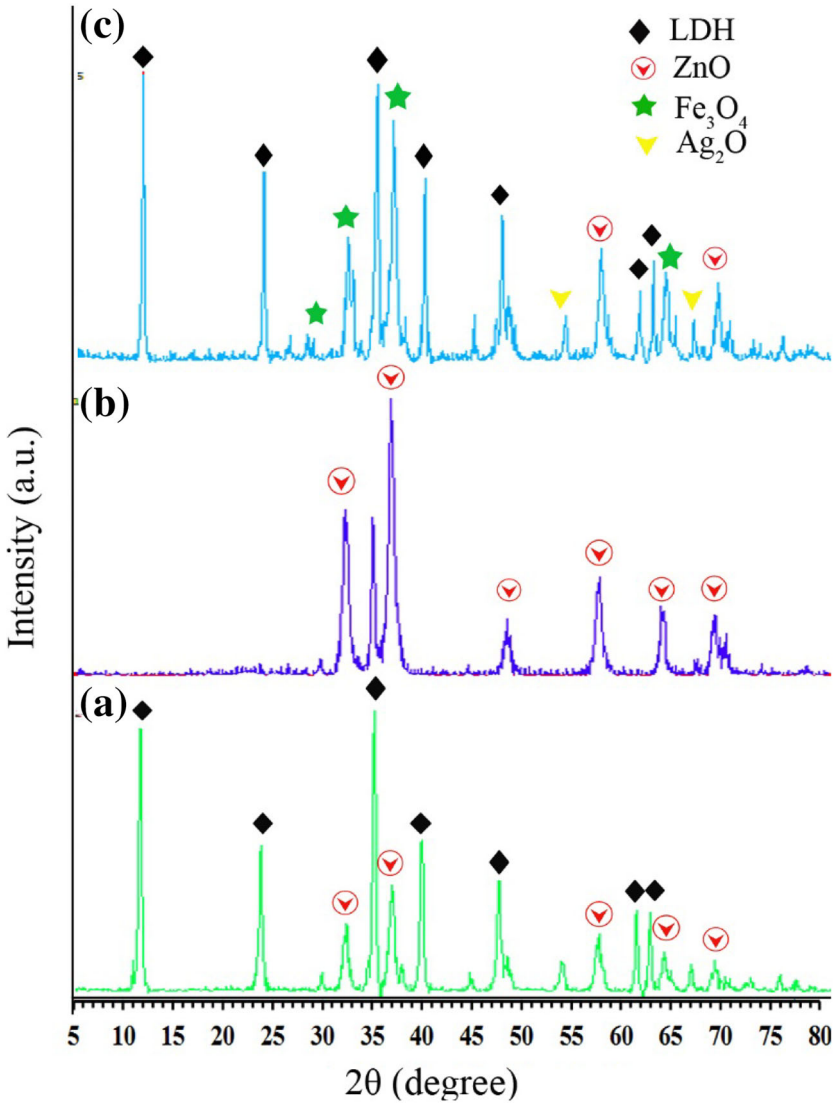

FIGURE 1 XRD patterns of (a) ZA-LDH, (b) LDO, and (c) $M_{10}A_5$-LDH

TABLE 1 Crystallographic parameters and textural properties of as-synthesized samples

Sample	$d_{(110)}$	$a^{[a]}$ (nm)	$D^{[b]}_{hkl}$ (nm)	Surface area ($m^2\ g^{-1}$)	Pore vol. ($cm^3\ g^{-1}$)	Pore size (nm)
ZnAl LDH	1.536	0.307	18	26	0.337	51
LDO 500	1.533	0.306	30	41	0.37	36
$M_{10}A_5$-LDH	-	-	15	39	0.38	39

[a] $a = 2 \times d_{110}$.
[b] Crystallite size based on the Scherrer equation.

with no cations leaching during the reconstruction process.[30] Moreover, the crystalline size of the samples calculated using the Scherrer equation is given in Table 1.

The adsorption–desorption isotherms of ZA-LDH, LDO, and $M_{10}A_5$-LDH samples could be attributed to the surface area and the pore structure.[38] As shown in Figure 2, both samples belong to Type IV isotherms with H3 hysteresis loops at high p/p_0, which is related to the mesopore size distribution. The structure fits pores with slit-shaped from the aggregation of LDH sheets.[39] Although the particle size distribution of the LDH and photocatalyst has a wide range, the LDO is more concentrated around 10 nm. Moreover, the specific surface areas and pore volume and size of the ZnAl LDH, LDO 500, and $M_{10}A_5$-LDH were obtained from the Barrett–Joyner–Halenda (BJH) theory and the data summarized in Table 1. It is noteworthy that the surface area of the mixed metal oxide (LDO) is more extensive than LDH

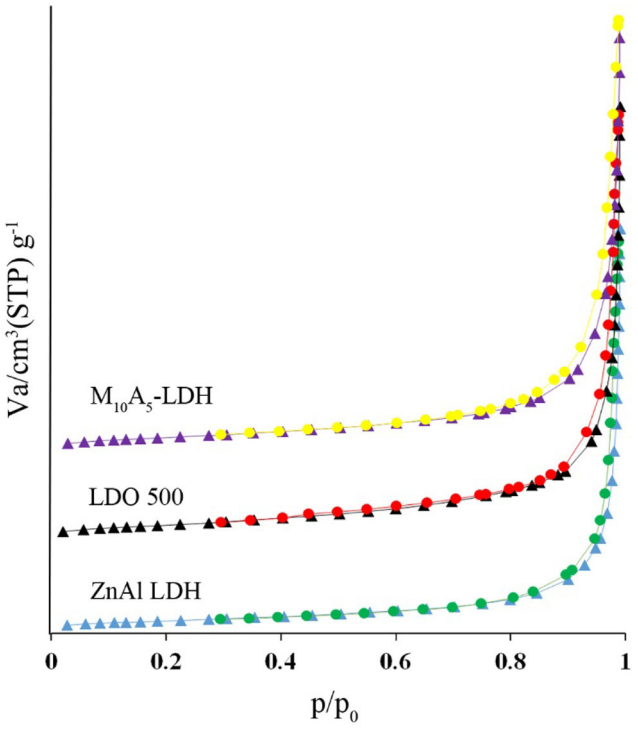

FIGURE 2 N_2 adsorption–desorption isotherms of different samples

due to the LDH sheet's collapse after thermal treatment. Besides, as it was predictable, the surface area of $M_{10}A_5$-LDH was larger than the LDH, and the reason is the surface area of the Fe_3O_4 and Ag_2O nanoparticles. The comparison of the surface area and the pore structure of all the samples shows a larger surface area, more significant pore volume, and smaller pore size for composite, which leads to an increase in photocatalytic activity of the catalyst.

The surface morphology and size distribution of the LDH and photocatalyst were investigated using scanning electron microscopy (SEM) (Figure 3). The SEM images of ZnAl-LDH (Figure 3a–c) delineated hexagonal shape with blunt edges and smooth surface, which constructed many nano-sheet-like particles with an average thickness of about 27 nm. Figure 3d–f clearly shows the even distribution of spherical particles of Fe_3O_4 and Ag_2O with a particle size around 20–30 nm on the plate of the LDH and reformation of crystalline structure. In other words, there was no considerable surface structure change after the reconstruction of LDH sheets and the addition of metal oxides owing to the memory effect of hydrotalcite. Furthermore, the EDS spectrum and the corresponding elemental mapping of the samples confirmed the

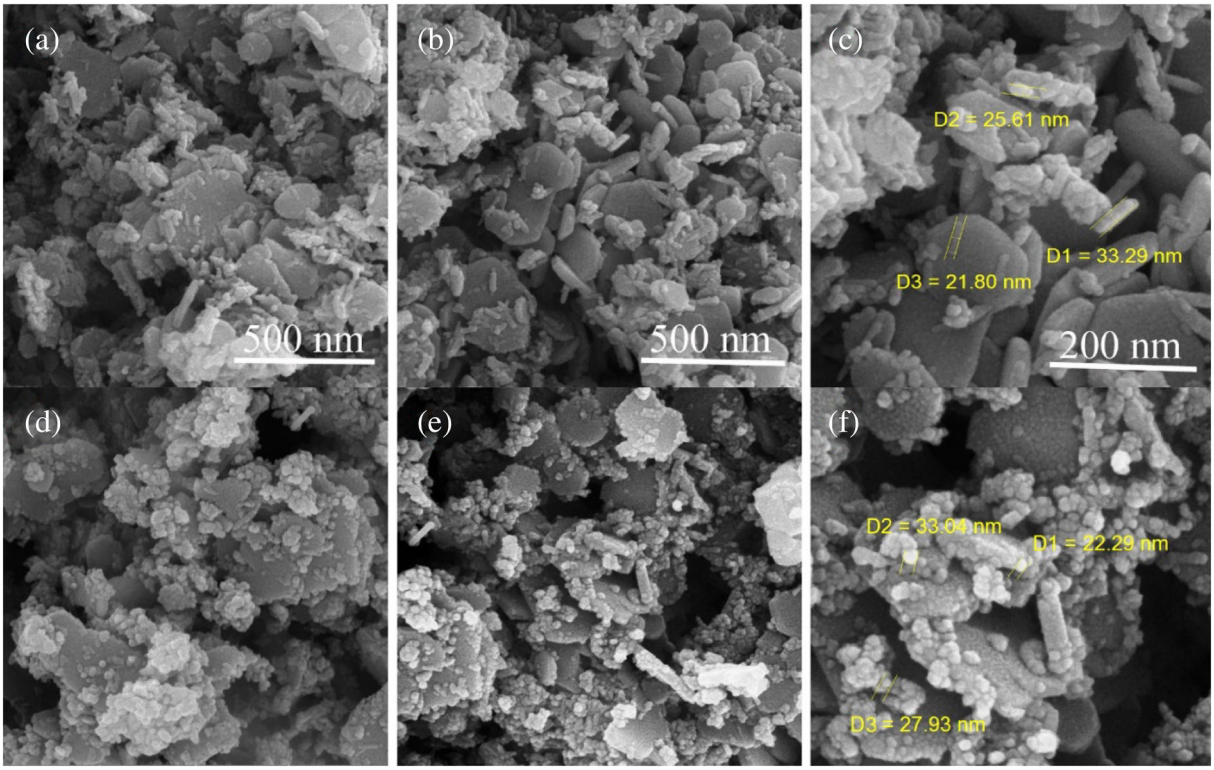

FIGURE 3 FE-SEM results of (a–c) ZA-LDH and (d–f) $M_{10}A_5$-LDH

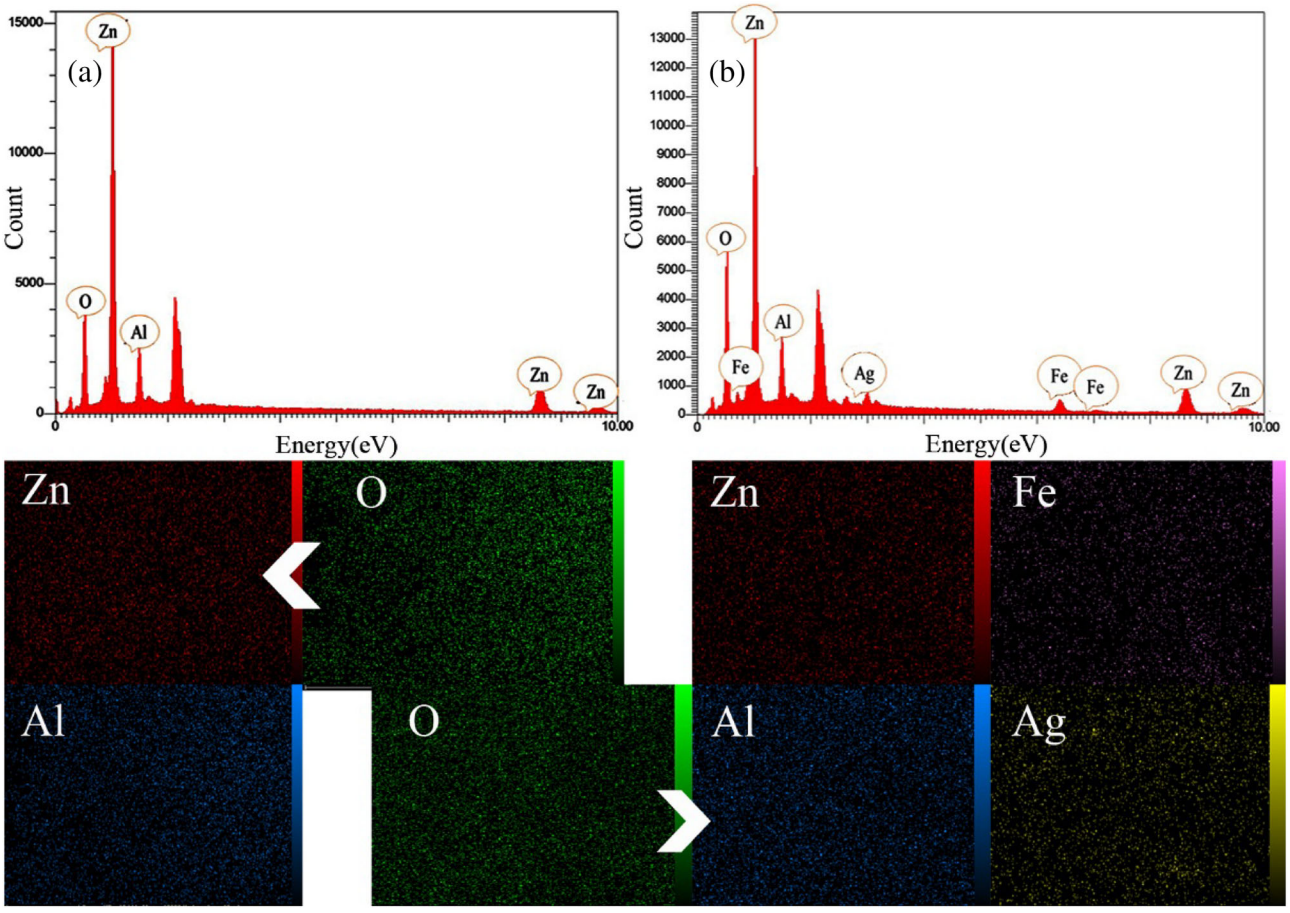

FIGURE 4 EDX spectra and elemental mapping of (a) ZA-LDH and (b) $M_{10}A_5$-LDH

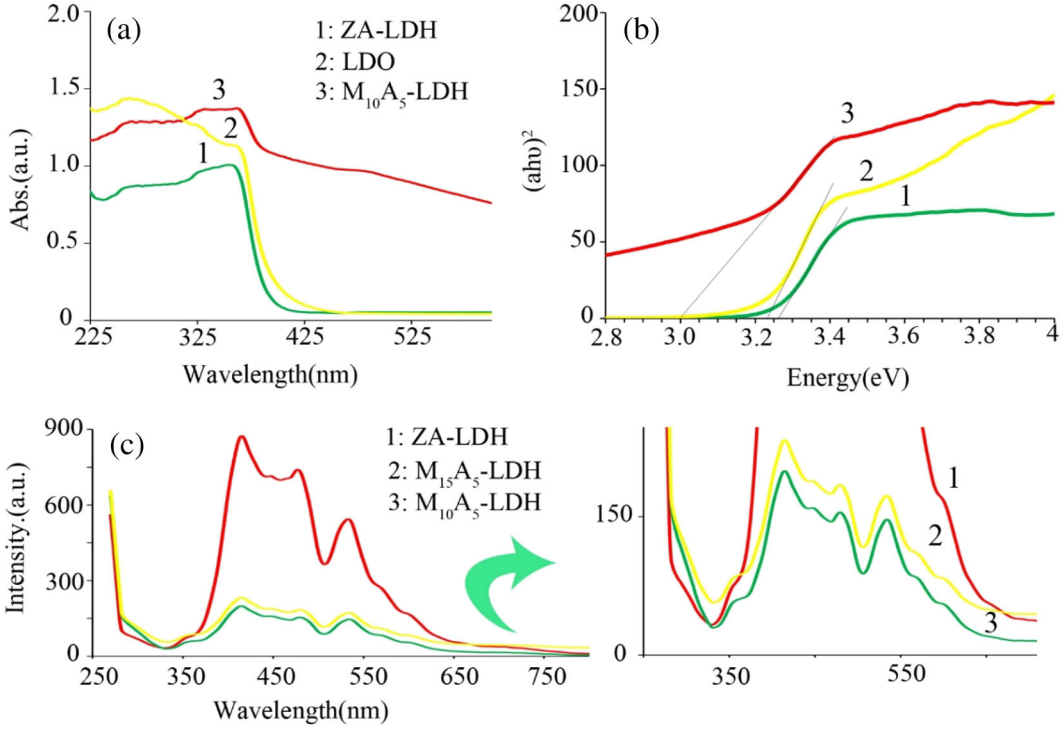

FIGURE 5 (a) UV–vis DRS results, (b) Tauc plot, and (c) PL graph of as-prepared samples

existence of Zn, Al, and O with the atomic percentage of 29.1, 9.1, and 61.7 as the essential parts of LDH (Figure 4a) and, in addition, Ag and Fe in the composition of $M_{10}A_5$-LDH (Figure 4b). As shown, the amount of Zn is about threefold of the Al element that agrees with the Zn: Al mole ratio of 3:1. In addition, the weight percentages of the Fe and Ag elements in the optimal photocatalyst are 1.9 and 1.7, respectively. As it can be seen from both elemental mapping and EDS spectrum, the oxygen concentration increased in composite due to the presence of magnetite. The EDS elemental mapping pictured the uniform distribution of all the elements, which affects the catalytic performance of the photocatalyst.

For further depth investigation to show improvement in photocatalytic capabilities of the composites in comparison with ZnAl-LDH, the optical and electrical behavior of the prepared samples was studied.

The optical absorption of the photocatalyst is a determinative property in the photodegradation procedure. Hence, the light absorption performance of the LDH, LDO, and $M_{10}A_5$-LDH has been examined through the solid-state UV–vis diffuse absorption spectra, and results were represented in Figure 5a. In the case of ZA-LDH, an adsorption edge appeared around 360 nm, and the absorption band is limited to the UV domain. The absorption edge of LDO shifted toward a higher wavelength but still occurred below the visible region. After hybridizing the ZA-LDH with a certain amount of Ag and magnetite, the composite presents a broad and robust light response in the UV–visible whole area, which reveals the synergistic effect between the LDH and metal oxides. These significant interactions could enhance photon absorption capacity. Also, extension in the light absorption range in composite raises the possibility of effective and sufficient utilization of the visible light absorption and improves photocatalytic behavior. Based on the Tauc plot (Figure 5b), the optical direct band gap energy for LDH found to be 3.21 eV, which is a consequence of the electronic transition from the O2p state to the metal ns or np levels for Zn (n = 4) and Al ($n = 3$).[40] The calculated band gap for composite decreased to 3.0 eV, which is mainly originated from the narrower band gap of Fe_3O_4 and the SPR effect of Ag species.[41,42] The broader light adsorption region refers to the intensified potential of $M_{10}A_5$-LDH to harvest the visible light in comparison to absolute LDH.

The PL analysis represents the efficiency of charge transfer and recombination process of electron–hole pairs in the interfaces of photocatalyst, which is the most critical factor in photocatalyst activity.[43] As is well known, the PL intensity is negatively related to photocatalytic activity.[44] It can be observed in Figure 5c that the ZA-LDH displays a wide, intense fluorescence emission peak at ~450 nm, which is related to different inherent defects, like interstitials and vacancies of zinc and oxygen.[45] On the contrary, the PL spectrum of composites was quenched and appeared much lower than LDH that shows good electrical conductivity of Fe_3O_4 and Ag_2O and SPR effect of Ag species.[46] On the other hand, the hybridization of LDH with these metal oxides caused the efficient separation of photoinduced charge carriers and decreased their recombination. Thus, it can affect the photodegradation efficacy of the resulting composites.

Moreover, the comparison between the PL spectrum of composites with 10% and 15% of magnetite revealed higher activity of $M_{10}A_5$-LDH. A proper explanation could be that the excess Fe_3O_4 nanoparticles could adversely accelerate the electron–hole recombination and diminish the charge separation.[47]

To further shed light on the synergistic effect between LDH and Ag_2O and Fe_3O_4, TPC response of ZA-LDH and $M_{10}A_5$-LDH was recorded (Figure 6). Based on TPC curves, both samples showed a periodic increase and decrease in current density by every switch on and off. Under UV–vis light, both pure ZA-LDH (Figure 6a) and composite (Figure 6b) produced repeatable responses, which show stability of the samples. The composite electrode photocurrent (1.05 μA) was about three times higher than that of the pure LDH electrode (0.35 μA), indicating enhanced mobility and photogenerated separation efficiency charge carriers as a result of the electronic interaction between LDH sheets and metal oxide

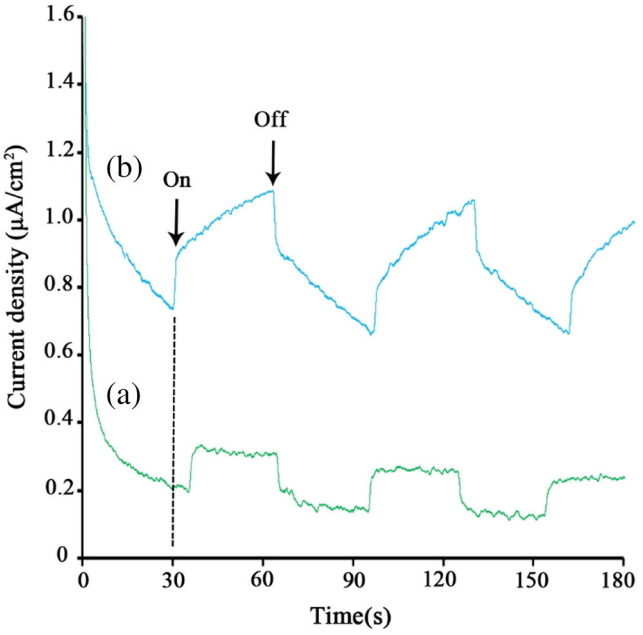

FIGURE 6 Photocurrent response of (a) ZA-LDH and (b) $M_{10}A_5$-LDH

nanoparticles. In total, this analysis proved the role of proper amounts of Ag_2O and magnetite semiconductors and constructive interactions of them and LDH in charge transition. On the other hand, the TPC of the LDH shows a delay in response when the light is switch on, which is a sign of the low sensitivity toward the light.

3.2 | Photodegradation of 4-NP

The strength of photocatalysts in photodegradation of PNP was evaluated by monitoring the change in the intensity of absorbance corresponding to the $\lambda = 400$ nm (Figure 7a).[48] By the elapse of irradiation time, the intensity of absorbance peak at λ_{max} decreased, which can be related to the mineralization of PNP molecules. No other peaks were observed at the end of the process, which confirms the degradation of PNP molecules in the presence of visible light irradiation. Under the dark condition, the blank test implied the relatively low adsorption capacity of the catalyst and also the impossibility of the degradation process in the absence of light. The curve of the blank sample increased during 60–120 min and then got stable till 180 min, which implies the completion of adsorption–desorption equilibrium of PNP on the catalyst. Although the LDH shows catalytic power for degradation of PNP aqueous solution, decomposition efficiency was 52% in 180-min reaction, whereas composites exhibited higher catalytic activity (72%–93%). The enhanced catalytic activity of $M_{10}A_5$-LDH in comparison with $M_{15}A_5$-LDH is in alignment with PL results, which explained that the higher activity of composite with 10% magnetite is a result of the best amount of Fe_3O_4 as the recombination center of electron–hole pairs (Figure 7b).

By considering the abovementioned results, $M_{10}A_5$-LDH was used as an optimum catalyst to investigate the impact of different amounts of catalyst in the photodegradation of PNP. Figure 7c shows the plot for the extent of decomposition (C/C_o) versus the time of light irradiation of PNP solution for 0.1, 0.15, 0.20, and 0.25 g of the photocatalyst. The photodegradation reached the maximum degree by the increase of photocatalyst dosage. Due to that, 0.25 g of the photocatalyst is considered the optimum amount. This phenomenon is related to the more active photogenerated species when a higher catalyst dosage was used. Using different initial concentrations of PNP solution revealed similar changes in C/C_o for 5 and 10 ppm of the sample. When the PNP concentration raised to 15 ppm, the degradation efficiency descended considerably to 74%. Higher concentrations of pollutants contain more molecules that consume the produced

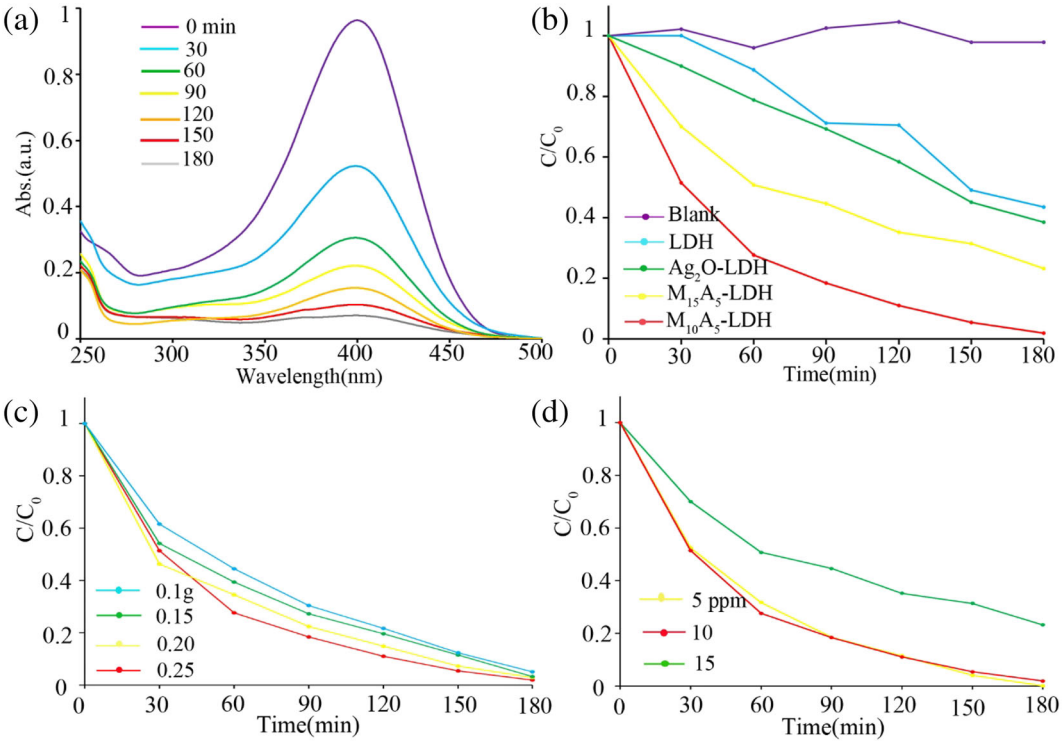

FIGURE 7 (a) UV–vis spectra depicting the degradation of PNP in the presence of $M_{10}A_5$-LDH, (b) photocatalytic performance of different samples, (c) the effect of the amount of catalyst, and (d) the effect of PNP concentration

active radicals faster and disturb the visible light utilization by the photocatalyst.[49] Therefore, 10 ppm accounted for the optimum concentration (Figure 7d).

To obtain more in-depth insight into the PNP photodegradation aspects in the presence of photocatalysts, investigation of the kinetic behaviors is in demand. The best representation for photocatalytic degradation of 4-NP in the pseudo-first-order mechanism ($-\ln [C_t/C_o] = kt$) is known as the Langmuir–Hinshelwood (L–H) mechanism.[50,51] According to this model, the apparent rate constant (k) was calculated for LDH, $M_{10}A_5$-LDH, and $M_{15}A_5$-LDH (Figure 8a). All R^2 correlation coefficients were higher than 0.95, which indicates model conformity. The k values were gradually increased from pure LDH to the composites, and the k values of the $M_{10}A_5$-LDH composite (0.020 min^{-1}) are fourfold higher than ZA-LDH (0.005 min^{-1}).

Additionally, to compare the PNP photodegradation activity in the presence of various photocatalysts, some previously reported works are summarized in Table 2. To be able to reach the catalyst performances, degradation efficiency, which is the amount of PNP (mg) per the dosage of catalyst (g) per the time of the reaction (h), was represented for each photocatalyst. Although all of these catalysts can degrade PNP solution to high percentages, they all have degradation efficiency much lower than the photocatalyst presented in this work. Moreover, another advantage of the $M_{10}A_5$-LDH composite is its excellent performance under irradiation of sunlight simulator lamps, whereas the other reported catalysts need special UV or visible light sources.

The photocatalyst performance, after it recycles a couple of times, is a critical factor for the practical application of catalysts. The reusability of the $M_{10}A_5$-LDH was evaluated by its photodegradation proficiency and the outcomes depicted in Figure 8b. The reuse examination showed that the photocatalyst could be reused up to five cycles without a considerable decrease in degradation efficiency toward PNP. The photocatalytic degradation efficiency declined from 98% in the first use to about 70% in the fifth cycle. The reduction in the activity of the $M_{10}A_5$-LDH probably returns to the leaching of Ag_2O nanoparticles or weight loss during the separation and washing process of the catalyst from the degraded

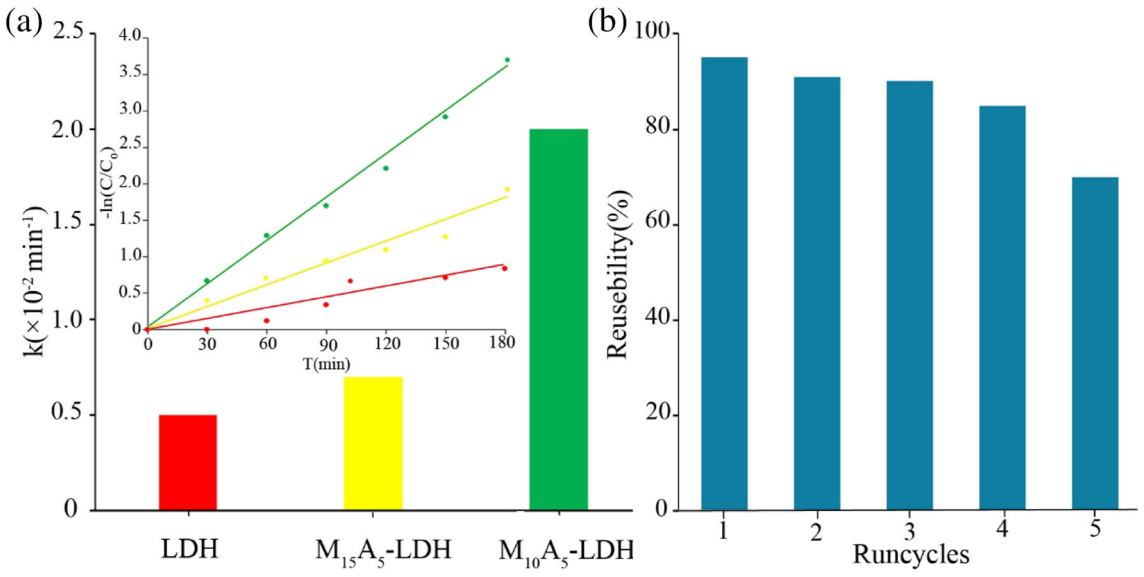

FIGURE 8 (a) Comparison of k values and kinetics of different samples and (b) reusability of the $M_{10}A_5$-LDH catalyst for PNP photodegradation

TABLE 2 Comparison of reported LDH-based photocatalysts for the degradation of PNP reported in the literature

Catalyst	Light source	Degradation efficiency (mg pollutant/g-catalyst.h)	Degradation (%)	Ref.
Zn-Ni-Al LDO	Visible	3.03	93	[52]
Pt-Ag/Zn_2Al	UV–vis	2.77	71	[30]
Fe_2O_3/ZnAlFe LDH	UV	2.31	100	[37]
yP-LDH_500CN	Visible	2.50	98	[48]
$M_{10}A_5$-LDH	UV–vis	13.33	93	This work

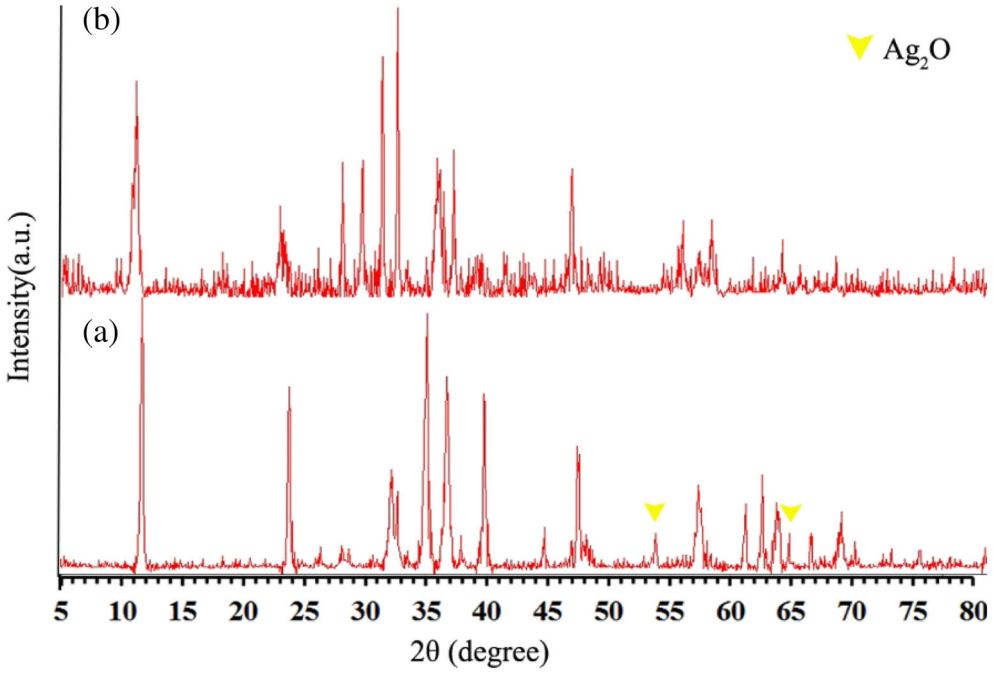

FIGURE 9 XRD patterns of $M_{10}A_5$-LDH catalyst (a) before usage and (b) after five-cycle usage

solution. Additionally, the XRD pattern remains unchanged after five cycles of photodegradation (Figure 9), indicating that the nanostructure of catalyst, spatially Ag_2O content, remains stable. It is concluded that the $M_{10}A_5$-LDH composite has good stability and reusability.

3.3 | Investigation of photodegradation mechanism

To further explore the influence of different scavengers on the photodegradation reaction, benzoquinone (BQ), iso-propanol (i-PrOH), and potassium iodide (KI) (all in 1 mM concentration) were chosen for trapping the active radicals ($\bullet O_2^-$, •OH, and h^+) in the medium of the reaction in the presence of $M_{10}A_5$-LDH. Based on comparison with the blank test (without scavenger), the PNP degradation percentage significantly decreased from 93% to 17%, and the rate constant dropped 10 times by the addition of KI, implying that h^+ was the prominent active radical. Furthermore, BQ and i-PrOH also decreased the PNP degradation ratio to 68% and 31%, respectively, signifying that $\bullet O_2^-$ and •OH are the less influential species in the degradation process (Figure 10). Relying on the results of this examination, the possible mechanism for the visible light-assisted degradation of PNP over $M_{10}A_5$-LDH composite was depicted in Figure 11. Essentially, among all of the involved semiconductors in composite, Ag_2O (1.2 eV) and Fe_3O_4 (2.0 eV) are active in the visible region of the light, and so, they can be excited by the

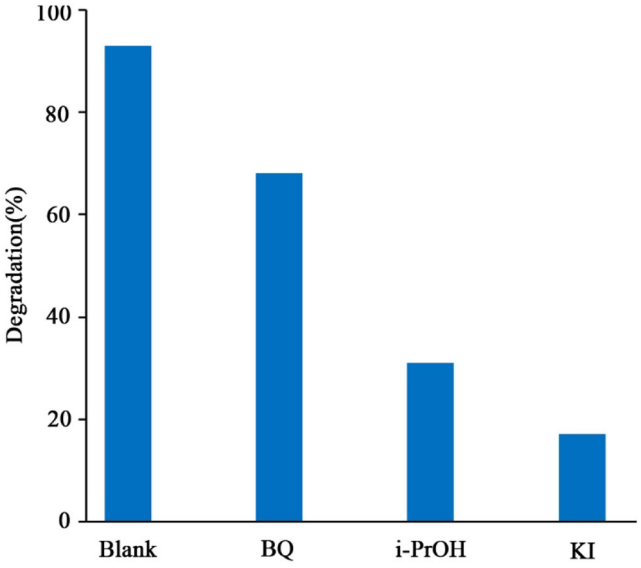

FIGURE 10 The effect of different radical scavengers on PNP photodegradation by $M_{10}A_5$-LDH

used radiation source.[53,54] Both embedded Ag_2O and magnetite on the LDH can respond to the visible light by photogeneration of electron–hole pairs, despite the LDH having no electron transfer under visible light.[55–57] Meanwhile, some of the photogenerated electrons at the conduction band (CB) energy level of Ag_2O (+0.2 eV)[58] could transfer to the CB of Fe_3O_4 and then CB of ZnAl LDH instantly and create a hole in the valence band (VB) of Ag_2O. This charge separation process causes stabilization and thus hinders the recombination process.

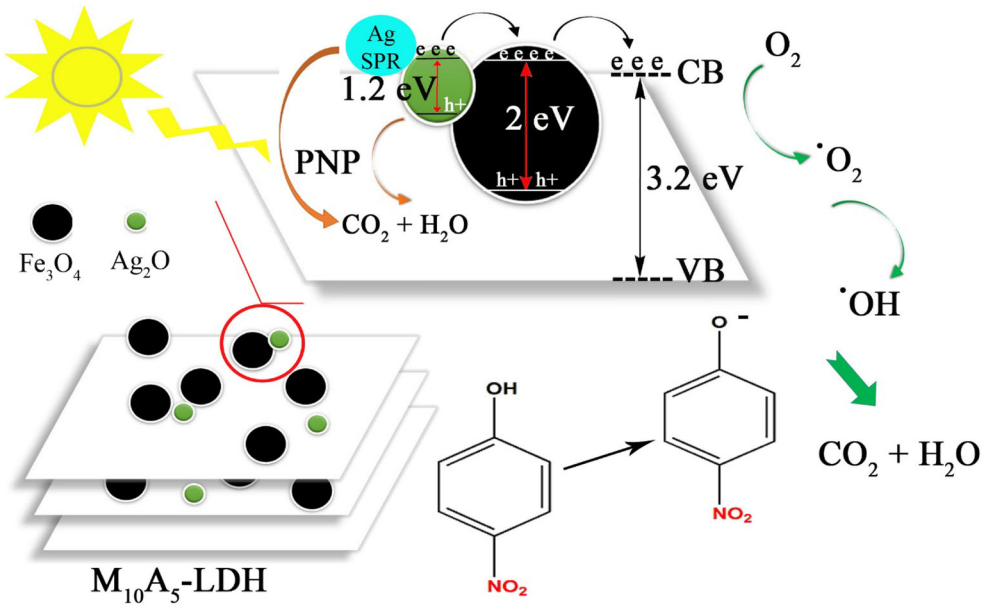

FIGURE 11 Charge transfer mechanism in PNP photodegradation

Hence, ZnAl-LDH as an n-type semiconductor indirectly responds to visible light and transfers the received electron to the dissolved oxygen to form $\bullet O_2^-$ radicals and •OH, respectively, by combining with water. Besides, extra •OH can be released by the reaction between the facial OH^- groups on the LDH and produced holes.[59] Because the CB potential of Ag_2O (+1.4 eV)[54] is higher than the standard redox potential of $\bullet OH/H_2O$ (+2.68 eV),[60] the holes on the VB of Ag_2O cannot produce •OH.[61] Therefore, they would react with PNP and oxidize the adsorbed contaminations directly. On the other hand, from the partial photoreduction of Ag_2O during the photocatalytic process, Ag° species can form, which can absorb more visible light photons due to the surface plasma resonance of Ag° species.[41] By the significant role of h^+ and other active radicals (•OH and $\bullet O_2^-$), the PNP ion efficiently breaks down into different organic intermediate molecules. Next, it produce more simple organic acids and ultimately mineralize them into CO_2 and H_2O. Released NO_2^- groups also oxidize by •OH species to nitrates.[11]

4 | CONCLUSION

A facile and eco-friendly method was applied to synthesize magnetic photocatalysts based on LDH. The $M_{10}A_5$-LDH photocatalyst was synthesized by considering the essential factors in photocatalytic activity, including interlayer anion in LDH, calcination temperature of LDH, and amount of Ag_2O and magnetite. The uniform distribution of metal oxides on LDH and synergistic effect between them enhanced the charge separation in the composite, which was demonstrated through FE-SEM, PL, and photocurrent response tests of the $M_{10}A_5$-LDH. This catalyst efficiently decreased the PNP concentration to 93% in 180 min and degradation efficiency up to 13.33 mg PNP/g-catalyst.h under irradiation of visible light by following pseudo-first-order kinetic. Above all, the photocatalyst recovered quickly by an external magnet and was used again for five cycles, maintaining relatively good execution. Using scavenger agents revealed that the most operative species in the photodegradation process is h^+. Moreover, The ZnAl-LDH as a platform improved the charge transfer from Ag_2O and Fe_3O_4 and thus produced active radicals for degradation of PNP. This catalyst has the potential to be testified in photodegradation and even photoreduction of different kinds of contaminants.

ACKNOWLEDGMENTS

We wish to express our gratitude to the Research Affairs Division Isfahan University of Technology (IUT), Isfahan, for partial financial support.

AUTHOR CONTRIBUTIONS

Mohammad Dinari: Conceptualization; data curation; formal analysis; funding acquisition; supervision; validation; visualization. **Firooze Dadkhah:** Data curation; formal analysis; investigation; methodology; software; validation.

CONFLICT OF INTEREST

The authors stated that there are no conflicts of interest in this work.

DATA AVAILABILITY STATEMENT

Data are available on request from the authors.

ORCID

Mohammad Dinari https://orcid.org/0000-0001-5291-7142
Firooze Dadkhah https://orcid.org/0000-0003-4616-5209

REFERENCES

[1] R. Fatima, M. N. Afridi, V. Kumar, J. Lee, I. Ali, K.-H. Kim, J.-O. Kim, *J. Clean. Prod.* **2019**, *231*, 899.
[2] Y.-X. Yao, H.-B. Li, J.-Y. Liu, X.-L. Tan, J.-G. Yu, Z.-G. Peng, *J. Nanomater.* **2014**, *2014*.
[3] M. Aghaei, A. H. Kianfar, M. Dinari, *Appl. Organomet. Chem.* **2020**, *34*, e5617.
[4] S. Zhang, W. Sun, L. Xu, X. Zheng, X. Chu, J. Tian, N. Wu, Y. Fan, *BMC Microbiol.* **2012**, *12*, 1.
[5] D. Rajamanickam, M. Shanthi, *Arabian J. Chem.* **2016**, *9*, S1858.
[6] D. S. Babu, V. Srivastava, P. Nidheesh, M. S. Kumar, *Sci. Total Environ.* **2019**, *696*, 133961.
[7] S. Asadzadeh-Khaneghah, A. Habibi-Yangjeh, *J. Clean. Prod.* **2020**, *276*, 124319.
[8] A. Habibi-Yangjeh, S. Asadzadeh-Khaneghah, S. Feizpoor, A. Rouhi, *J. Colloid Interface Sci.* **2020**, *580*, 503.
[9] M. Muruganandham, R. P. Suri, M. Sillanpää, J. J. Wu, B. Ahmmad, S. Balachandran, M. Swaminathan, *J. Nanosci. Nanotechnol.* **2014**, *14*, 1898.
[10] S. Naraginti, F. B. Stephen, A. Radhakrishnan, A. Sivakumar, *Spectrochim. Acta, Part A* **2015**, *135*, 814.
[11] P. Xiong, Y. Fu, L. Wang, X. Wang, *Chem. Eng. J.* **2012**, *195*, 149.
[12] M. Cantarella, A. Di Mauro, A. Gulino, L. Spitaleri, G. Nicotra, V. Privitera, G. Impellizzeri, *Appl. Catal. B* **2018**, *238*, 509.
[13] A. Bhattacharjee, M. Ahmaruzzaman, *RSC Adv.* **2016**, *6*, 41348.
[14] M. Dinari, M. M. Momeni, Z. Bozorgmehr, S. Karimi, *J. Iran. Chem. Soc.* **2017**, *14*, 695.
[15] B. Luo, G. Liu, L. Wang, *Nanoscale* **2016**, *8*, 6904.
[16] M. Dinari, M. M. Momeni, Y. Ghayeb, *J. Mater. Sci. Mater. Electron.* **2016**, *27*, 9861.
[17] E. Seftel, M. Puscasu, M. Mertens, P. Cool, G. Carja, *Appl. Catal. B* **2015**, *164*, 251.
[18] P. F. Liu, S. Yang, B. Zhang, H. G. Yang, *ACS Appl. Mater. Interfaces* **2016**, *8*, 34474.
[19] W.-K. Jo, Y.-G. Kim, S. Tonda, *J. Hazard. Mater.* **2018**, *357*, 19.
[20] D. Chen, Y. Li, J. Zhang, W. Li, J. Zhou, L. Shao, G. Qian, *J. Hazard. Mater.* **2012**, *243*, 152.
[21] W. Du, Y. Xu, Y. Wang, *Langmuir* **2008**, *24*, 175.
[22] D. Malwal, P. Gopinath, *Cat. Sci. Technol.* **2016**, *6*, 4458.
[23] J. Yang, H. Chen, J. Gao, T. Yan, F. Zhou, S. Cui, W. Bi, *Mater. Lett.* **2016**, *164*, 183.
[24] A. Radoń, A. Drygała, Ł. Hawełek, D. Łukowiec, *Mater. Charact.* **2017**, *131*, 148.
[25] D. Petrov, R. Ivantsov, S. Zharkov, D. Velikanov, M. Molokeev, C.-R. Lin, C.-T. Tso, H.-S. Hsu, Y.-T. Tseng, E.-S. Lin, *J. Magn. Magn. Mater.* **2020**, *493*, 165692.
[26] M. Xu, L. Han, S. Dong, *ACS Appl. Mater. Interfaces* **2013**, *5*, 12533.
[27] F. Rezaei, M. Dinari, *Colloids Surf.* **2021**, *618*, 126441.
[28] A. Haghighi, M. Haghighi, M. Shabani, S. G. Fard, *J. Hazard. Mater.* **2020**, 124406.
[29] W. Shen, X. Wang, Y. Ge, H. Feng, L. Feng, *Colloids Surf.* **2019**, *575*, 102.
[30] M. Darie, E. M. Seftel, M. Mertens, R. G. Ciocarlan, P. Cool, G. Carja, *Appl. Clay Sci.* **2019**, *182*, 105250.
[31] M. J. Barnabas, S. Parambadath, A. Mathew, S. S. Park, A. Vinu, C.-S. Ha, *J. Solid State Chem.* **2016**, *233*, 133.
[32] M. Dinari, F. Dadkhah, *Carbohydr. Polym.* **2020**, *228*, 115392.
[33] F. Rodriguez-Rivas, A. Pastor, C. Barriga, M. Cruz-Yusta, L. Sánchez, I. Pavlovic, *Chem. Eng. J.* **2018**, *346*, 151.
[34] K. Yang, L.-g. Yan, Y.-m. Yang, S.-j. Yu, R.-r. Shan, H.-q. Yu, B.-c. Zhu, B. Du, *Sep. Purif. Technol.* **2014**, *124*, 36.
[35] K. Abderrazek, F. S. Najoua, E. Srasra, *Appl. Clay Sci.* **2016**, *119*, 229.
[36] G. Huang, Y. Sun, C. Zhao, Y. Zhao, Z. Song, J. Chen, S. Ma, J. Du, Z. Yin, *J. Colloid Interface Sci.* **2017**, *494*, 215.
[37] E. Seftel, M. Puscasu, M. Mertens, P. Cool, G. Carja, *Catal. Today* **2015**, *252*, 7.
[38] N. Gibson, P. Kuchenbecker, K. Rasmussen, V.-D. Hodoroaba, H. Rauscher, Volume-specific surface area by gas adsorption analysis with the BET method, in *Characterization of Nanoparticles*, (Eds: V.-D. Hodoroaba, W. E. S. Unger, A. G. Shard), Elsevier, Amsterdam, The Netherlands **2020** 265.
[39] X. Tao, D. Liu, W. Cong, L. Huang, *Appl. Surf. Sci.* **2018**, *457*, 572.
[40] G. Huang, J. Chen, D. Wang, Y. Sun, L. Jiang, Y. Yu, S. Ma, Y. Kang, *Mater. Lett.* **2016**, *173*, 227.
[41] Z. Zhu, Z. Lu, D. Wang, X. Tang, Y. Yan, W. Shi, Y. Wang, N. Gao, X. Yao, H. Dong, *Appl. Catal. B* **2016**, *182*, 115.
[42] H. Yin, K. Yu, C. Song, R. Huang, Z. Zhu, *ACS Appl. Mater. Interfaces* **2014**, *6*, 14851.
[43] M. K. Seery, R. George, P. Floris, S. C. Pillai, *J. Photochem. Photobiol., A* **2007**, *189*, 258.
[44] B. Song, Z. Zeng, G. Zeng, J. Gong, R. Xiao, S. Ye, M. Chen, C. Lai, P. Xu, X. Tang, *Adv. Colloid Interface Sci.* **2019**, *272*, 101999.
[45] H. Mou, C. Song, Y. Zhou, B. Zhang, D. Wang, *Appl. Catal. B* **2018**, *221*, 565.
[46] B. Xu, Y. Li, Y. Gao, S. Liu, D. Lv, S. Zhao, H. Gao, G. Yang, N. Li, L. Ge, *Appl. Catal. B* **2019**, *246*, 140.
[47] Y. Zhu, R. Zhu, G. Zhu, M. Wang, Y. Chen, J. Zhu, Y. Xi, H. He, *Appl. Surf. Sci.* **2018**, *433*, 458.
[48] X. Li, Z. Yu, L. Shao, H. Zeng, Y. Liu, X. Feng, *J. Hazard. Mater.* **2020**, *386*, 121650.
[49] L. Hu, S. Dong, Y. Li, Y. Pi, J. Wang, Y. Wang, J. Sun, *J. Taiwan Inst. Chem. Eng.* **2014**, *45*, 2462.
[50] Z. Li, Q. Zhang, X. Liu, M. Chen, L. Wu, Z. Ai, *Appl. Surf. Sci.* **2018**, *452*, 123.
[51] K. Zhang, Y. Liu, J. Deng, S. Xie, H. Lin, X. Zhao, J. Yang, Z. Han, H. Dai, *Appl. Catal. B* **2017**, *202*, 569.
[52] G. Zhang, L. Hu, R. Zhao, R. Su, Q. Wang, P. Wang, *J. Photochem. Photobiol., A* **2018**, *356*, 633.
[53] H. El Ghandoor, H. Zidan, M. M. Khalil, M. Ismail, *Int. J. Electrochem. Sci* **2012**, *7*, 5734.
[54] D. Zhang, S. Cui, J. Yang, *J. Alloys Compd.* **2017**, *708*, 1141.

[55] A. N. Shafawi, R. Aliah Mahmud, K. Ahmed Ali, L. Kurnianditia Putri, N. I. Md Rosli, A. R. Mohamed, *J. Photochem. Photobiol., A* **2020**, *389*, 112289.

[56] R. Aliah Mahmud, A. Natasha Shafawi, K. Ahmed Ali, L. Kurnianditia Putri, A. R. Mohamed, *Mater. Res. Bull.* **2020**, *128*, 110876.

[57] N. I. Md Rosli, S. M. Lam, J. C. Sin, I. Satoshi, A. R. Mohamed, *J. Environ. Eng.* **2018**, *144*, 04017091.

[58] X. Wang, S. Li, H. Yu, J. Yu, S. Liu, *Chem.–A Eur. J.* **2011**, *17*, 7777.

[59] L. Mohapatra, K. Parida, *J. Mater. Chem. A* **2016**, *4*, 10744.

[60] D. A. Armstrong, R. E. Huie, W. H. Koppenol, S. V. Lymar, G. Merényi, P. Neta, B. Ruscic, D. M. Stanbury, S. Steenken, P. Wardman, *Pure Appl. Chem.* **2015**, *87*, 1139.

[61] X. Yuan, W. Li, *Appl. Clay Sci.* **2017**, *138*, 107.

How to cite this article: M. Dinari, F. Dadkhah, *Appl Organomet Chem* **2021**, e6355. https://doi.org/10.1002/aoc.6355